Journal of Hydrology, 110 (1989) 87–105
Elsevier Science Publishers B.V., Amsterdam — Printed in The Netherlands

PREFERENTIAL SOLUTE TRANSPORT IN LAYERED HOMOGENEOUS SANDS AS A CONSEQUENCE OF WETTING FRONT INSTABILITY

ROBERT J. GLASS, GERKE H. OOSTING and TAMMO S. STEENHUIS

Department of Agricultural and Biological Engineering, Cornell University, Ithaca, NY 14853 (U.S.A.)

(Received June 28, 1988; accepted after revision January 2, 1989)

ABSTRACT

Glass, R.J., Oosting, G.H. and Steenhuis, T.S., 1989. Preferential solute transport in layered homogeneous sands as a consequence of wetting front instability. J. Hydrol., 110: 87–105.

Laboratory solute transport experiments were carried out in layered homogeneous sand with a fine textured layer overlying a coarse layer. Pulses of blue dye are used to characterize the solute movement. Unlike the traditionally expected one-dimensional homogeneous flow, the solute moves in preferred paths or "fingers" induced by infiltration flow instability starting at the textural interface between the fine and the coarse layer. The effect of repeated long term ponded infiltration cycles, intermittent ponding events and of uniform initial moisture content at field capacity on the flow field structure and solute breakthrough curves is studied. The possibility of using a simple lumped dispersion coefficient that includes additional mixing processes due to instability is explored and implications for field solute transport monitoring practices are discussed.

INTRODUCTION

Over the past twenty to thirty years the application of solute transport theory, based on laboratory soil column experiments, to field situations has been increasingly questioned. There is a growing realization that the one-dimensional flow observed in homogeneous laboratory columns (Bodman and Colman, 1943) does not adequately describe field solute transport. This should not be surprising as more than a century ago, Lawes et al. (1882) found that a large portion of water added to a soil only slightly interacted with that already present in the root zone. Yet, the one-dimensional, homogeneous flow model still forms the basis of conventional models currently in use (Carsel et al., 1985; Leonard et al., 1986; Nofziger and Hornsby, 1986; Jury et al., 1987; Steenhuis and Naylor, 1987.

Research supported by EPA grant R-812919-01-1: "Wetting front instability in layered soils and its inclusion in monitoring and modeling techniques" and USDA Hatch funding through the Agricultural Experiment Station.

0022-1694/89/$03.50

At present, research on heterogeneous flow in the field can be divided into two approaches: statistical and phenomenological. The statistical approach concentrates on measuring and describing the variability of solute travel times. The distribution of solute travel times obtained from intensive random sampling of an individual field is superimposed on the one-dimensional homogeneous flow model. This approach may yield a good prediction of the transport of pollutants to the water table under a particular field if the structure of the solute transport variability is adequately represented. However, in order to do this, intensive sampling must be done for each field in question, a time-consuming and expensive undertaking.

The phenomenological approach consists of defining and describing the mechanisms that cause heterogeneous flow and their incorporation into modeling and monitoring practices. Two mechanisms which cause highly nonuniform solute transport have been identified, one involving movement in isolated channels or macropores such as cracks or earthworm holes (e.g., Beven and Germann, 1982; Smettem and Collis–George, 1985; Richard and Steenhuis, 1988) and another due to the phenomenon of wetting front instability, also termed "fingering".

Current field evidence (Starr et al., 1986; Glass et al., 1988; Van Ommen et al., 1988) has shown that wetting front instability can cause nonuniform solute transport in soils whose hydraulic conductivity increases with depth but does not vary markedly from point to point horizontally. In these soils, water and solutes can move through "fingers" to groundwater at speeds approaching the saturated pore velocity of the subsoil under unit gradient. In addition, laboratory experimentation has documented the persistence of fingers from infiltration cycle to infiltration cycle and the effect of porous media properties on finger width and velocity (Glass et al., 1987).

In this paper, we present the results of experiments designed to study wetting front instability in soils where a fine textured layer overlies a coarser layer. We demonstrate the effect of repeated steady infiltration cycles, intermittent ponding events and uniform initial moisture content at field capacity on both wetting front instability and solute transport. Solute transport itself gives information about wetting front instability and the interaction of persisting fingers or "core" regions with surrounding less wet "fringe" regions. Such persistence and interaction have implication for field solute transport modeling and for monitoring practices.

EXPERIMENTAL METHOD

A two-dimensional unstable flow field was generated in a Plexiglas chamber 1 cm thick, 51 cm wide and 140 cm high. The chamber was filled with two layers of sand, the top layer being much finer than the bottom layer. On one side of the chamber about 100 holes allowed air to escape freely. The holes were small enough to prevent sand from escaping but large enough that water never entered them during an experiment. White silica sand, used commercially for

TABLE 1

Experiments conducted

Experiment run number	Initial moisture condition	Begin time of pulse (h)	Flow rate (mm min^{-1})	t_p^* (min)
$1A_1$	Dry	4	4.26	24.5
$1A_2$		24	4.09	25.5
$1B_1$	1 day after 1A	4	3.91	54.0
$1B_2$		24	3.32	62.0
$1B_{int}$	1 day after 1B	0	0.027	3420.0
$2A_1$	Dry	4	4.19	25.5
$2A_2$		24	4.11	25.5
$2A_3$		48	3.93	25.5
$2B_1$	1 day after 2A	4	3.93	41.0
$2B_2$		24	4.07	43.0
$2B_3$		48	3.87	47.0
$2B_{int}$	1 day after 2B	0	0.027	3120.0
$2C_1$	1 day after $2B_{int}$	4	3.92	60.5
$2C_2$		24	3.65	65.5
$2C_3$		48	3.77	60.5

* Time of peak concentration

sand blasting, was sieved through US sieve series numbers 14, 40 and 200. The 14–40 fraction was used for the coarse bottom layer while that which passed the 200 sieve constituted the top fine layer. The sands were cleaned and dried before and between uses to assure purity. The chamber was filled with the bottom sand layer through a funnel–extension–randomizer assembly to minimize segregation and heterogeneities and then packed using a drop impact method. After packing, at least 10 cm of the top of the coarse sand layer was removed to bring the bottom layer thickness to 129 cm. The bulk density of the bottom layer was approximately 1.5 g cm^{-3} yielding a porosity of 42%. After making the textural interface as flat as possible, the fine top layer was added and tamped 1 cm at a time until it was 8 cm thick. Sand cleaning and chamber filling and packing procedures were described in detail in Glass (1985).

The experiments carried out are summarized in Table 1. Two replicates (numbered 1 and 2) of three consecutive infiltration experiments (A, B, B_{int}) were conducted in which the initial moisture distribution was varied systematically. A fourth infiltration experiment (C) was not replicated. Distilled water with a constant low nonadsorbing dye concentration (0.025% solution of USDA Red no. 3) was used in all of the experiments so that the water could easily be seen. In each infiltration experiment pulses of USDA blue no. 1 dye solution (approximately 0.058%) were used to characterize the solute movement. Pulses were added by allowing the ponding level to decrease from 1.5 to 1 cm after which 25.5 ml of the blue dyed water was mixed thoroughly in the ponded water. Constant ponding to a level of 1.5 cm was resumed just as all blue dyed water

had moved into the top layer. The subscripted number in the experiment label refers to the blue pulse number.

In the first infiltration experiment of the two replicates (1A and 2A), the sand was initially air dry. A depth of 1.5 cm of water was ponded and maintained for 72 h during which solute pulses were added at 4, 24 and 48 h. The chamber was then sealed at the top to inhibit evaporation and allowed to drain by gravity for 24 h. The moisture content field at the end of the drainage cycle formed the initial moisture field for the second experiment.

The second infiltration experiment (replicates 1B and 2B) was then conducted with a steady ponding level of 1.5 cm for 72 h again with solute pulses at 4, 24 and 48 h. After 24 h drainage of this "B" experiment, 1.5 cm of water was added every 8 h for a two week period with the first 1.5 cm containing the solute. This third experiment, simulating intermittent irrigation events, we denote by "B_{int}" following the replicate number.

The fourth (and final) experiment (C) was only carried out during replicate 2. In preparation for this experiment the bottom layer in the chamber was saturated several times, sealed and drained for another 24 h. A uniform moisture content of about 6% in the bottom layer resulted. This final experiment was again conducted with a steady ponding level of 1.5 cm for 72 h with solute pulses at 4, 24 and 48 h and is denoted by "2C". In this way the first (A) and fourth (C) experiments represented the initial moisture content conditions (i.e., uniform) often used in analytical and numerical studies of infiltration flows. The experiments in the B group mimic more realistic field situations where initial moisture content varies from point to point, and infiltration is either steady (B) or intermittent (B_{int}).

To measure the flow variability of both water and solute, the flow at the bottom of the chamber was measured through seventeen separate sections each having a width of 3 cm. These "drip sections" restricted the lateral movement of water at the bottom of the chamber and thus enabled the monitoring of the flow of both water and solute through individual fingers and its change in time. In addition, the movement of the solute through the chamber was easily visualized and documented with time lapse photography on movie film. Data was taken from the film by projecting it onto a screen and then tracing the wetting front position with time on acetate sheets.

Water was periodically collected from each drip section and the concentration of the blue dye in each sample was measured using the colorimetric method. A photospectrometer was used at a wavelength of 685 mm and a standard curve, relating transmittance to concentration, was determined at the time of each pulse through a series of standard solutions of known concentration.

RESULTS

Results of our experiments, are divided into two sections, flow field structure and solute breakthrough curves. The structure of the flow field is of great consequence for solute transport and is described in detail.

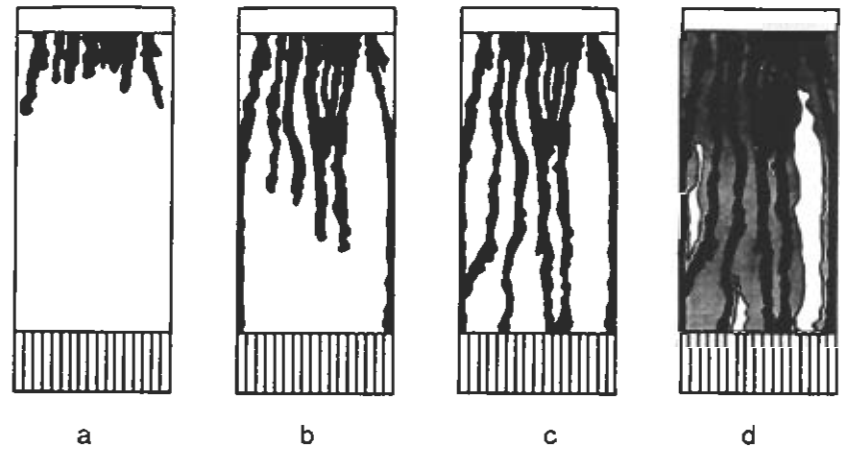

Fig. 1. Development of the finger core area–fringe area in time, for experiment 1A. Core areas grow from the textural interface downward to the bottom of the chamber within the first 30 min (a, b, c). Finger fringe areas are formed as wetting fronts leave the fingers and move laterally into the dry sand on either side of the finger core areas (d). This finger core and fringe structure persists into the B and B_{int} experiments.

Flow field structure

In all experiments, wetting front movement within the top fine layer was stable while instabilities occurred in the coarse bottom layer. In the initially dry sand (A experiment), water crossed into the coarse layer at many discrete points, each generating a small finger. Many of these then merged to form larger faster moving fingers which continued to move downward. These fingers persisted in time and formed "core" areas that conducted most of the flow through the chamber. Over time, slow sideways-moving wetting fronts passed from these finger core areas into the dry sand on either side of the finger, creating a surrounding "fringe" area. The fringe areas are at a much lower moisture content than the finger core areas and consequently conduct very little of the flow. Figure 1 is a drawing of finger development in the bottom layer of experiment 1A showing the rapid downward growth followed by a stage of slow lateral growth into the fringe areas.

Once the slow laterally moving wetting fronts had passed through all of the dry sand, very little change in flow field could be detected. The dramatic fringe and core region structure within the bottom coarse layer persisted for the duration of the 72 h infiltration cycle of experiment A.

Table 2 presents the number of final fingers, average width, average finger tip velocity and percent total area of the chamber occupied by fingers for the two replicates of the A experiment. The "average" structure appears to be very similar between the two replicates.

TABLE 2

Finger properties

Replicate number	Final number of fingers	Average width ± STD (cm)	% of chamber occupied by fingers	Average velocity ± STD (cm min^{-1})
1A	6	2.14 ± 0.50	25.2	6.51 ± 0.05
2A	6	1.59 ± 0.21	18.7	7.06 ± 1.75

At the start of the B experiment, 24 h after the water flow in the A experiment was stopped, the initial moisture content field appeared almost uniform to the eye. However, upon ponding in the B experiment, the fringe and core structure in the bottom layer again reappeared. The locations of the core regions as highlighted by the blue pulses were almost the same as in the A experiment. In general, however, the participation of the fringe areas in conducting water and solute increased over the A experiment, although the core regions continued to conduct the majority of the flow. In another experiment this structure of core and fringe has been documented to persist in excess of ten days (Glass, 1985).

In the subsequent B_{int} experiments where water was applied intermittently, the finger structure in the 30 cm directly below the textural interface was the same as in the ponded A and B experiments. Below this region the structure became more complicated and there was more merging of fingers. Essentially, three regions, one on each side and one in the middle, conducted the majority of the water and dye. The widths of the regions on the side were about 9 and 6 cm, while the middle region measured 20 cm.

In the final C experiment the moisture content was initially uniform. As the wetting front moved from the textural interface it became wavy, the amplitude of the wave increasing as it moved towards the bottom of the chamber. Such an

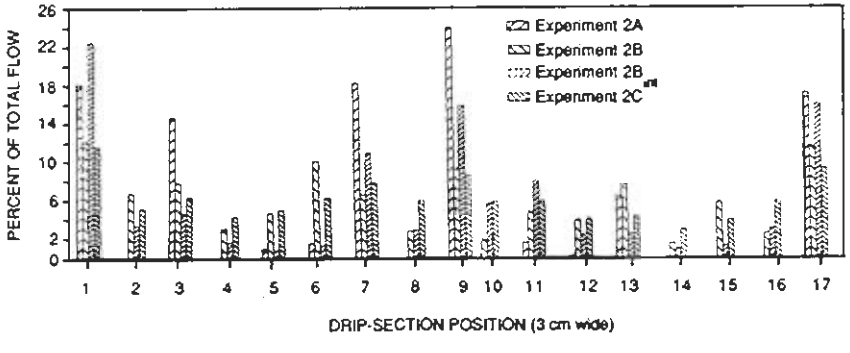

Fig. 2. Distribution of flow as sampled from the bottom of the chamber through the drip section. Flow is given for each location across the drip section as a percent of the total flow.

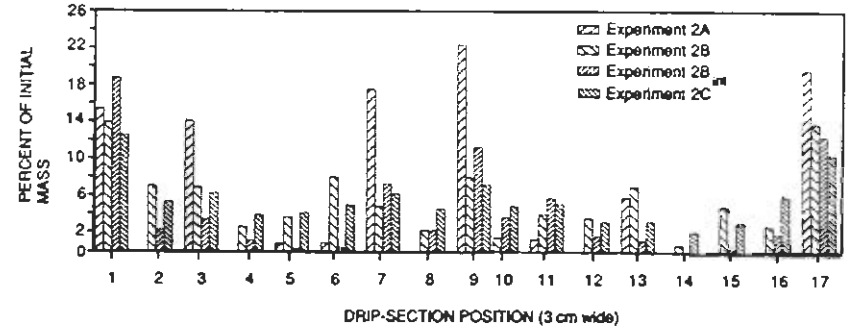

Fig. 3. Distribution of solute transport as sampled from the bottom of the chamber through the drip section. Percent of total solute mass applied through each drip section position is given.

increase in amplitude with depth is an indication of instability; however, the dramatic finger structure found in the A, B and B_{int} experiments was not present. Blue dye pulses showed an exaggeration of the wave form of the initial wetting front with a wide diffuse "core" area in the middle and along each side of the chamber. This flow field structure illuminated by the blue pulses changed little over the 72 h infiltration period.

Both the flow and the total solute mass distribution over seventeen drip sections at the bottom of the chamber for each of the A, B, B_{int} and C experiments can be used to show the extreme deviation from the homogeneous flow usually assumed for layered sands. For example, Fig. 2 presents the percent of the total flow for each drip section for the infiltration experiments in the second replicate and Fig. 3 the percent total mass transported through each drip section. As expected there is close agreement between the percent flow and the percent mass carried by a particular drip section. The standard deviation across the seventeen drip sections can be used as a measure of the uniformity of the flow field: the more uniform, the lower the standard deviation. The standard deviation decreases from the A to the B to the C experiment from 8.0 to 3.3 to 2.1 for the flow distribution and from 7.8 to 3.6 to 2.5 for the percent mass distribution. However, in experiment B_{int} the standard deviation essentially doubled from its value in the B experiment from 3.3 to 6.1 for the flow distribution and from 3.6 to 4.9 for the percent mass distribution.

Breakthrough curves

Total chamber breakthrough curves (BTC) showing the relative concentration, C/C_0 in time, where C is the solute concentration of the fluid exiting the bottom of the chamber and C_0 is the initial concentration, can be constructed from the data obtained from the individual drip sections over time. Figure 4 combines the BTC's for all pulses of the A, B, and C experiments of the second replication. All of the blue pulses had a slightly different initial concentration,

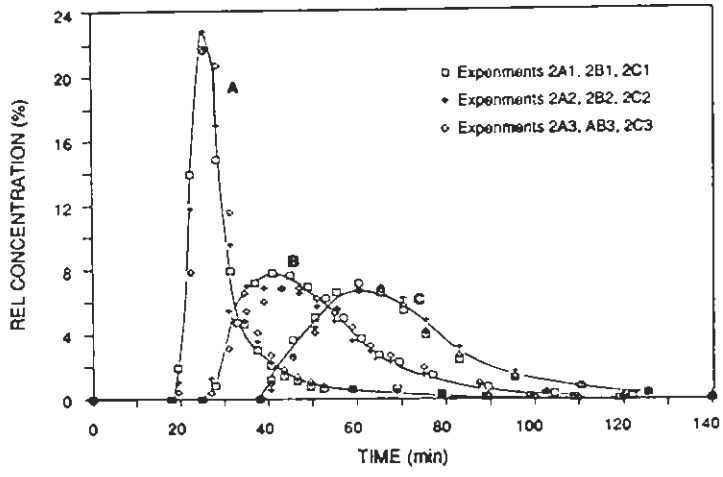

Fig. 4. C/C_0 vs. t(min) for the A, B and C experiments of the second replicate.

C_0, initial mass per unit area, M_0, and flow rate. In order to compare the BTC's precisely, we nondimensionalize time and plot a nondimensional form of the concentration which, when the integral over nondimensional time is taken, gives one. The nondimensional time, $t_\star$, is given as:

$$t_\star = Qt/Lf \tag{1}$$

where Q is the water flux through the chamber, t is the time, L is the total length from the top of the upper layer to the bottom of the lower layer, and f is the porosity of the bottom layer. The nondimensional solute or mass flux, $M_\star$, defined as:

$$M_\star = CLf/M_0 \tag{2}$$

has the property:

$$\int_0^\infty M_\star \, dt_\star = 1 \tag{3}$$

In this nondimensionalization we use the porosity, f, rather than the moisture content, θ, within the chamber, because θ varies substantially over the core–fringe structured flow field. Choice of an average moisture content in the chamber instead of f would equate nondimensional time to pore volume and we do this later. At this point however, use of f provides a proper nondimensionalization and allows comparison of all pulses.

Breakthrough curves presented in Fig. 4 for the "ponded" experiments of the second replicate are shown in nondimensional form in Fig. 5. A line is drawn

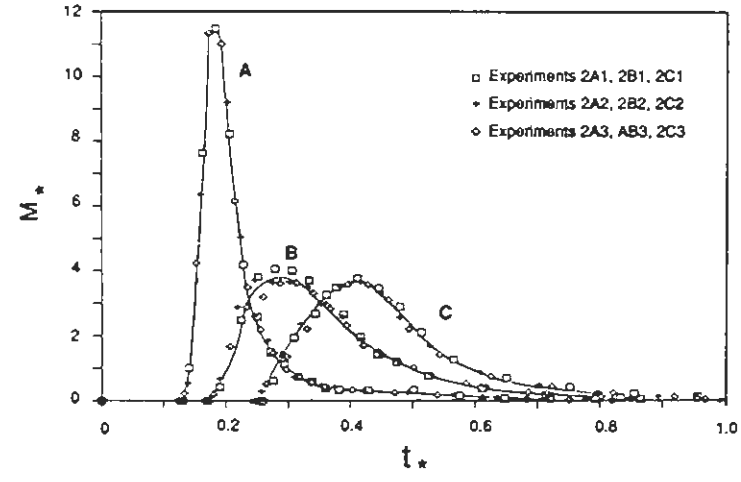

Fig. 5. $M_\star$ vs. $t_\star$ for the A, B and C experiments of the second replicate.

by hand through the data to better distinguish the three experiments. As can be seen from Fig. 5, the three breakthrough curves within each of the A, B and C experiments are almost identical and show no trend in time over the 72 h infiltration event. This, therefore, supports the visual impression that very little change in flow field structure occurred once the initial wetting fronts had moved through the chamber. In addition, reproducibility confirms that our experimental techniques were consistent and not responsible for the changes

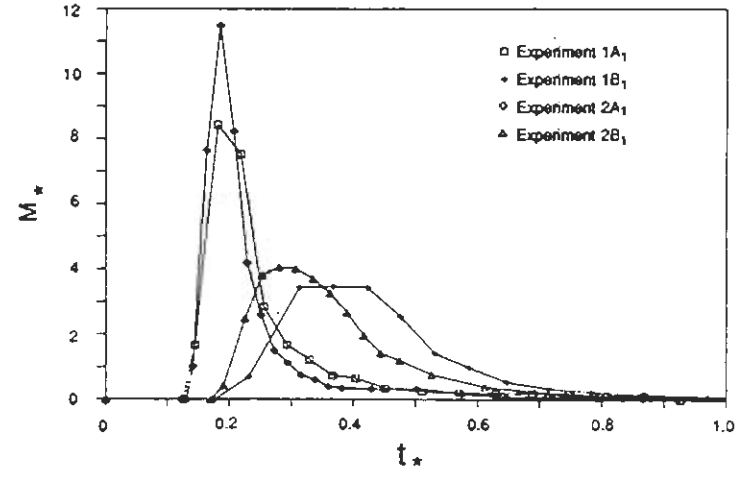

Fig. 6. Comparison of the breakthrough curves for the first pulses of replicates 1 and 2.

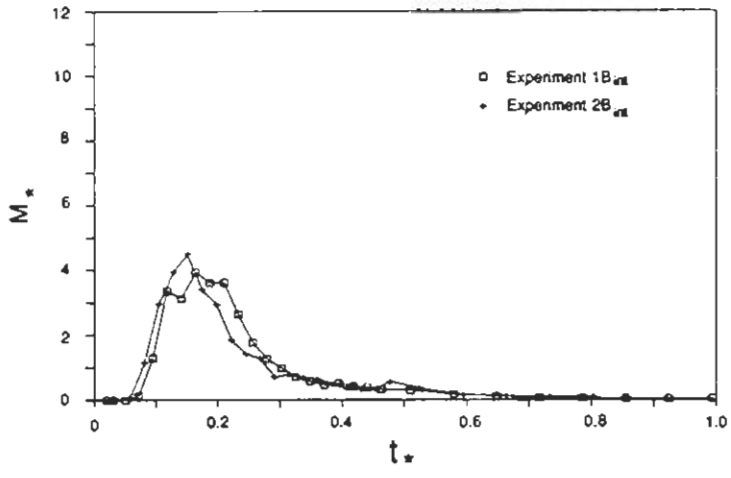

Fig. 7. Comparison of the breakthrough curves for experiments $1B_{int}$ and $2B_{int}$.

shape and position of the breakthrough curve as we progressed from the A to the C experiments.

The peak M_* and corresponding value of t_* decreases and increases respectively from the A through the C experiments. The very small effect of the fringe area in conducting water and solute in the A experiment is further emphasized by the fact that at the time of the first pulse, the laterally moving wetting fronts had yet to wet the entire chamber.

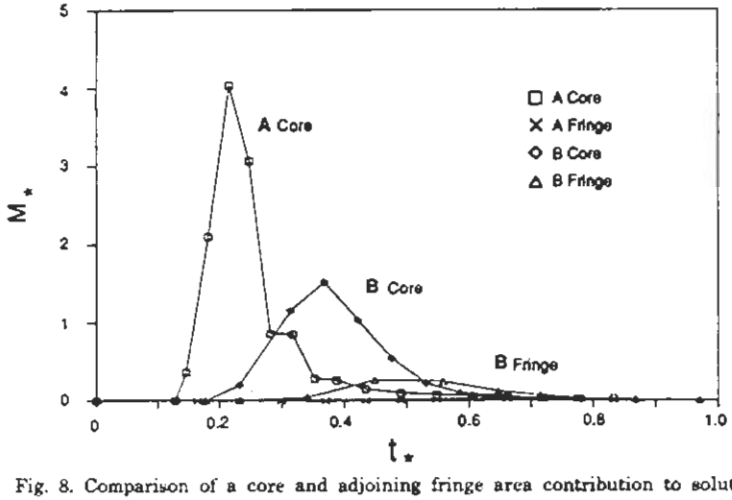

Fig. 8. Comparison of a core and adjoining fringe area contribution to solute transport in experiments $1A_1$ and $1B_1$.

Figure 6 shows a comparison of the first pulses in the A and the B experiments for each of the replicates ($1A_1$ and $2A_1$; $1B_1$ and $2B_1$). Since the initial flow field is unstable, the breakthrough curves would not be expected to be completely similar. However, Fig. 6 shows them to be remarkably alike, especially for the two replicates of the A experiment. This indicates that chamber scale structure of the flow field caused by the initial instability in a particular situation, may be similar without duplicating the individual fingers, their exact paths and interations.

The BTC's of the two replicates of the intermittent experiments ($1B_{int}$ and $2B_{int}$) are shown in Fig. 7. Again, we see a remarkable correspondence between the two. Comparison with Fig. 5 shows the peak M_* for the intermittent experiment to come through in nondimensional time before that of the A experiment. The B_{int} experiments were stopped after 70% of the total mass had moved through the chamber since the tail on the BTC was very long and our experimental time was limited. The final 30% of the mass would continue to "trickle" out at a very low concentration during a very long period.

The monitoring of water and mass flux out of the individual drip sections gives the opportunity to compare the contribution of the core and fringe structural regions. Figures 8 and 9 compare a core area with an adjoining fringe area. These two regions were selected because their flows could be easily separated. Figures 8 and 9 show the response of the core and fringe for the first pulses of the A and B experiments and the B_{int} experiment respectively. In the A experiment the contribution of the fringe area with its peak t_* at 0.7 is almost undetectable on the plot. For the B experiment the peak core area M_* decreases, the M_* distribution in t_* spreads out and the t_* at which the peak

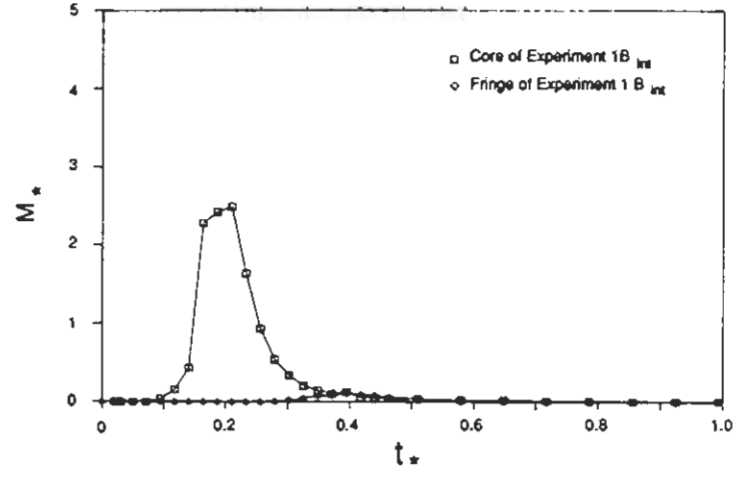

Fig. 9. Comparison of a core and adjoining fringe area contribution to solute transport in experiment $1B_{int}$.

M_* occurs shifts to the right. Alternatively, the B fringe areas peak M_* increases, and its t_* at which the peak M_* occurs shifts to the left. Thus, for the B experiments, the core and fringe areas, although very distinct, behave in a more similar way than in the A experiments. The B_{int} experiment reverses this trend with the peak separating further in both t_* and M_*.

Summary of experimental results

The effect of wetting front instability on the flow field structure and solute transport may be summarized as follows. In the A experiment, the flow field was very structured with large differences between core and fringe areas. The BTC's showed very early breakthrough with minimal enhanced mixing due to low core–fringe area interaction. In the B experiment, the flow field was less structured than the A experiment with less difference between core and fringe areas. While the BTC's showed early breakthrough, it was much later than in the A experiment. Interaction between core and fringe areas was enhanced causing greater mixing within the bottom layer. The B_{int} experiment exhibited a more complicated structure than the B or the A experiment. The interaction between core and fringe areas was much greater than in the previous two experiments and showed an earlier breakthrough in nondimensional time than did the A experiment. The C experiment demonstrated almost uniform flow with almost no structure. The BTC's from the C experiment can be viewed essentially as typically expected for homogeneous soil columns.

COMPARISON WITH ANALYTICAL SOLUTION ASSUMING HOMOGENEOUS FLOW

Many different approaches may be used to model solute transport through fingering flow fields. The purpose of this paper is to give a qualitative understanding of the phenomenon's effect on solute transport and its consequences for field scale modeling and monitoring practices. We chose, therefore, to apply the analytical solution most commonly used in many field scale solute transport models. In this way, we ignore our knowledge of the flow field structure and treat the vadose zone as if homogeneous with all the mixing processes — molecular diffusion, hydrodynamic dispersion, and complicated finger core and fringe region interaction — lumped into a common dispersion coefficient. Knowledge of the flow field structure and its incorporation into a more fundamental approach to modeling solute transport through fingering flow fields will be presented elsewhere.

For simplicity we chose the most uncomplicated analytic solution to the one-dimensional convection dispersion equation for the homogeneous situation. If we assume that the solute is applied in a band of infinitesimal thickness at the textural interface between the upper and lower layers; that above the textural interface the coarse sand extended upward indefinitely instead of the fine layer; and that the bottom boundary has no effect on water or solute movement then we have the solution:

$$C = \frac{M_0}{\theta_* (4\pi D t)^{1/2}} \exp\left\{\frac{-(x - vt)^2}{4Dt}\right\} \quad (4)$$

where D is the dispersion coefficient, x is the distance from textural interface, θ_* is the effective average moisture content within the bottom layer, v is the average pore velocity and $t = 0$ when the solute pulse just enters the coarse layer. This solution is used, for example, in the Model of Underground Solute Evaluation or MOUSE by Steenhuis et al. (1987). To apply eqn. (4), the dimensionless variables in eqns. (1) and (2) need to be redefined because of the change in the origin of the coordinate system and the need to include the effective average moisture content instead of the total porosity. By defining L_c as the length of the coarse layer and t_p as the time at which the peak C occurs at L_c, θ_* may be found as:

$$\theta_* = Q t_p / L_c \quad (5)$$

We also define a new dimensionless time, t_*, and mass flux, M_*, given by:

$$t_* = t/t_p = vt/L_c \quad (6)$$

and:

$$M_* = C L_c \theta_* / M_0 \quad (7)$$

Thus, we have:

$$M_* = \left[\frac{1}{4\pi D t_* / (L_c v)}\right]^{1/2} \exp\left[\frac{-(1 - t_*)^2}{4D t_* / (L_c v)}\right] \quad (8)$$

To apply eqn. (8) we translate $t_* = 0$ to the point where the pulse band is halfway across the textural interface. Equation (8) is then graphically fitted to the pulse data for the second replicate. The data for all pulses of a particular experiment are combined for the fit. The values of t_p, v, θ_* and the best fit for D are given in Table 3.

Figures 10 through 13 show the data and eqn. (8) plotted for the D-values chosen. The fit of eqn. (8) to the data appears to be fairly close. Equation (8), however, does not fit the falling side of the breakthrough curve, consistently

TABLE 3

BTC parameters

Experiment	Translated time to peak (min)	Q (mm min^{-1})	v (cm min^{-1})	D (cm^2 min^{-1})	θ_*	D/v (cm)
2A	16.3	4.07	7.94	40	0.0514	5.04
2B	34.6	3.94	3.73	42	0.1059	11.26
$2B_{int}$	2640.0	0.14	0.049	1.67	0.0571	34.08
2C	55.5	3.78	2.41	14	0.1567	5.81

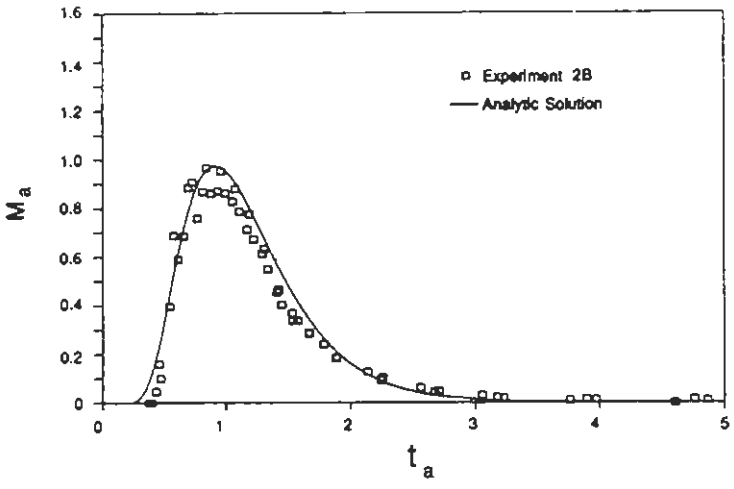

Fig. 10. Comparison of analytic solution with replicate 2A. Solid line is eqn. (8) with $D = 40\,\mathrm{cm^2\,min^{-1}}$, $L_c = 129\,\mathrm{cm}$ and $v = 7.94\,\mathrm{cm\,min^{-1}}$.

first overpredicting and then underpredicting M_a. This error is seen most dramatically for the B_{int} experiment (Fig. 12) where approximately 30% of the mass is yet to leave the column at $t_a = 5$, resulting in an extremely long tail.

The fact that eqn. (8) can be used to "predict" the majority of the BTC is not too surprising as the form of the BTC ignoring the tail is very similar to the

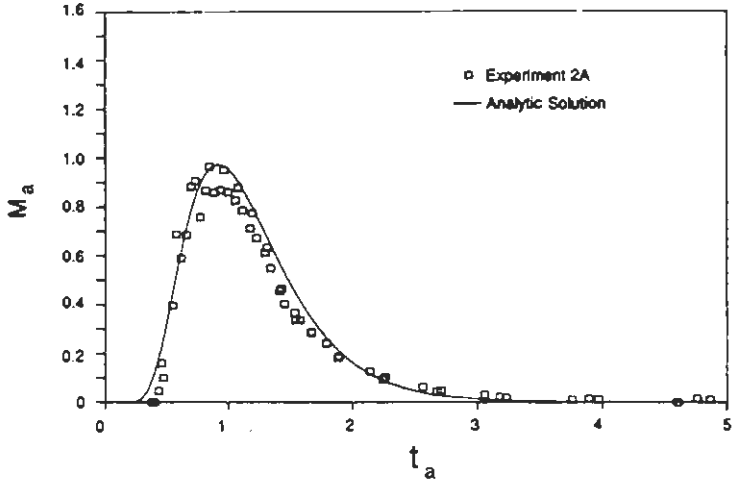

Fig. 11. Comparison of analytic solution with replicate 2B. Solid line is eqn. (8) with $D = 42\,\mathrm{cm^2\,min^{-1}}$, $L_c = 129\,\mathrm{cm}$ and $v = 3.73\,\mathrm{cm\,min^{-1}}$.

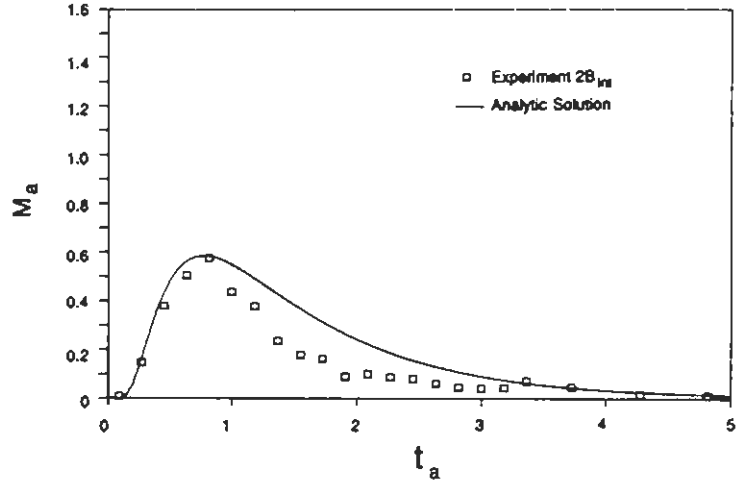

Fig. 12. Comparison of analytic solution with replicate $2B_{int}$. Solid line is eqn. (8) with $D = 1.67\,\mathrm{cm^2\,min^{-1}}$, $L_c = 129\,\mathrm{cm}$ and $v = 0.049\,\mathrm{cm\,min^{-1}}$.

form of eqn. (8); t_p is simply fit by the calculation $v = L/t_p$ and D is chosen to give the required spread. From this point of view, eqn. (8) is forced on the data and the dispersion coefficient is nothing more than a fitted parameter without much physical significance.

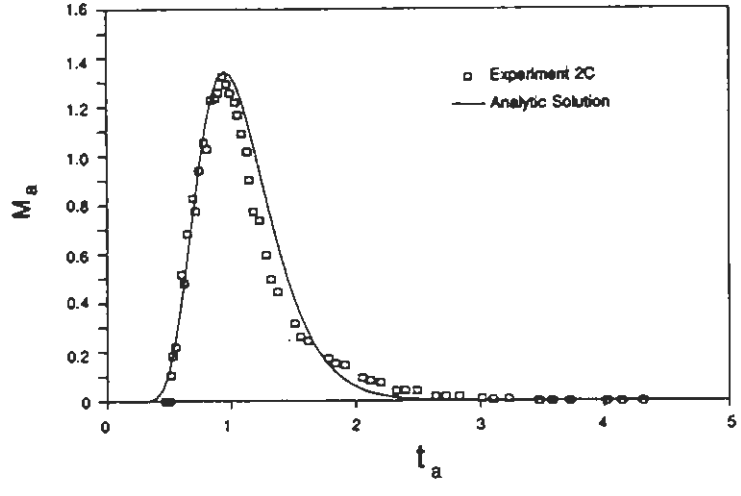

Fig. 13. Comparison of analytic solution with replicate 2C. Solid line is eqn. (8) with $D = 14\,\mathrm{cm^2\,min^{-1}}$, $L_c = 129\,\mathrm{cm}$ and $v = 2.41\,\mathrm{cm\,min^{-1}}$.

If molecular diffusion and hydrodynamic dispersion are the only mixing processes occurring, then in the range of Peclet numbers we have in our experiments, the quotient of dispersion coefficient and velocity is generally assumed to be a constant (Bear, 1972; van Genuchten and Wierenga, 1986). As can be seen from Table 3, D/v for the A and C experiments is essentially the same, (approximately 5 cm). This result emphasizes what we have already noted with respect to the flow field structure above. In the A experiment, interaction between core and fringe areas is very small so that water and solute essentially move only through the core areas while in the C experiment almost no core and fringe structure is present. Thus, core–fringe mixing processes do not affect solute transport in the A and C experiments and only diffusion and hydrodynamic dispersion are operating. In the B and B_{int} experiments, however, D/v increases by a factor of two and then seven respectively. This increase points to the role of core–fringe mixing interaction in the lumped chamber scale dispersion process and directly mirrors the level of interaction noted in the visual movement of the blue dye through the chamber.

Our physical understanding of flow through unsaturated porous media states that under the same potential gradient, the average pore velocity, v, increases with θ. However, θ_e doubles from the A to B and triples from the A to the C experiments. θ_e for the B_{int} is essentially the same as for the A experiment. Obviously, θ_e bears no physical resemblance to the actual moisture content within the chamber and has likewise become a curve fitting parameter. For the highly structured A experiment, we may make use of the flow field structure to reinterpret θ_e. If we take A_F, the cross-sectional area in fingers instead of A, we may calculate a θ_F, the average moisture content of the transporting core regions, of 0.28. θ_F is much higher than θ_e calculated to be 0.0514.

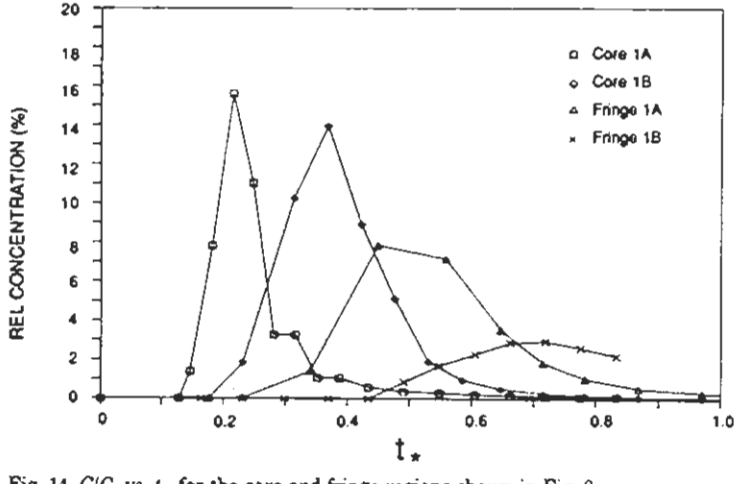

Fig. 14. C/C_0 vs. t_* for the core and fringe regions shown in Fig. 8.

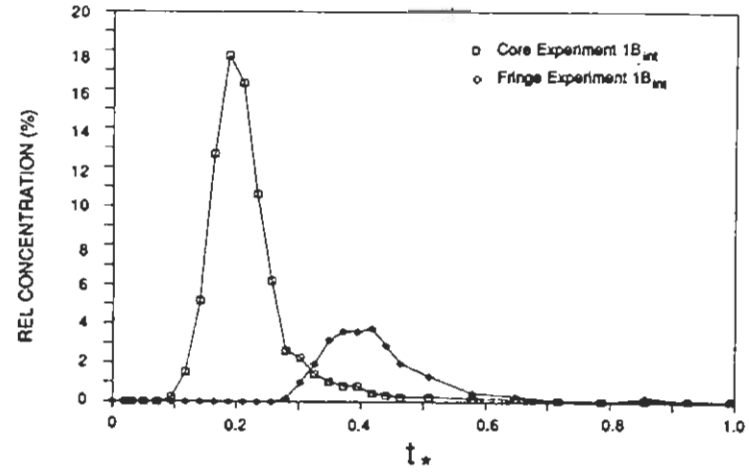

Fig. 15. C/C_0 vs. t_* for the core and fringe regions shown in Fig. 9.

IMPLICATIONS FOR FIELD MONITORING STRATEGIES

The best monitoring plan has usually been to sample solute travel times at enough points to adequately represent the solute transport time structure for the site. The number of these points is usually based on the structure of the variability of soil properties expected at the site. Since fingering is not linked to soil variability directly, such a monitoring approach in sandy soils will not adequately represent the solute transport travel time structure for the site and conventional models based on such incomplete data would be misleading. This is further illustrated by Figs. 14 and 15 in which the relative concentration, C/C_0, is plotted versus t_*. If the relative concentration was used as would normally be obtained from a soil core, the influence of the fringe area in solute transport would be much overestimated because the concentrations are not properly weighted by their flow rates. If fingers are missed entirely and only fringe areas are sampled, then misleading interpretations such as rapid degradation, volatilization or plant uptake could be made to account for the missing solute.

The complicated interactions in the B_{int} experiment, most like a field situation, emphasize the need for sampling techniques that integrate the flow over a large enough region to sample several core and fringe regions. Such a technique is proposed by Starr and Parlange (1986) and consists of sampling the capillary fringe of the groundwater with suction lysimeters. This method shows promise since water flow in the capillary fringe region is still vertical and fingers will widen and coalesce under high uniform moisture content.

CONCLUSION

Wetting front instability has great influence on solute transport through fine over coarse sand systems. The formation of fingers due to the instability within the homogeneous bottom layer in a first infiltration cycle causes a rapid breakthrough of solute and a decrease in the volume of porous medium available for chemical interaction. In subsequent steady infiltration cycles, persisting fingers continue to cause early solute breakthrough, however, complicated core–fringe interaction may effectively double the apparent dispersion through the system. Intermittent infiltration most closely approximating the natural field condition increases the apparent dispersion by a factor of seven and causes an extremely long tail on the breakthrough curve. Such complicated mixing processes in even a homogeneous porous medium demonstrate the severe difficulty faced in modeling solute transport or planning a solute monitoring program in the vadose zone.

REFERENCES

Bear, J., 1972. Dynamics of Fluids in Porous Media. Elsevier, New York, N.Y., 764 pp.

Beven, K. and Germann, P., 1982. Macropores and water flow in soils. Water Resour. Res., 18: 1311–1325.

Bodman, G.B. and Colman, E.A., 1943. Moisture and energy conditions during downward entry of water into soils. Soil Sci. Soc. Am., Proc. 8: 116–122.

Carsel, R.F., Mulkey, L.A., Lorber, M.N. and Baskin, L.B., 1985. The pesticide rootzone model (PRZM): A procedure for evaluating pesticide leaching threats to groundwater. Ecol. Modeling 30: 49–69.

Glass, R.J., 1985. A study of wetting front instability in layered porous media. M.Sc. thesis, Dep. of Agric. Eng., Cornell University, Ithaca, N.Y.

Glass, R.J., Parlange, J.-Y. and Steenhuis, T.S., 1987. Water infiltration in layered soils where a fine textured layer overlays a coarse sand. Proc. Int. Conf. Infiltration Dev. Appl., Hawaii, pp. 66–81.

Glass, R.J., Steenhuis, T.S. and Parlange, J.-Y., 1988. Wetting front instability as a rapid and far-reaching hydrologic process in the vadose zone. J. Contam. Hydrol., 3: 207–226.

Jury, W.A., Focht, D.D. and Farmer, Q.J., 1987. Evaluation of pesticide groundwater pollution potential from standard indices of soil–chemical adsorption and biodegradation. J. Environ. Qual., 16: 422–428.

Lawes, J.B., Bilbert, J.H. and Warington, R., 1882. On the Amount and Composition of the Rain and Drainage Waters Collected at Rothamsted. Clowes, London.

Leonard, R.A., Knisel, W.G. and Still, D.A., 1986. GLEAMS: Groundwater loading effects of agricultural management systems. ASAE Paper No. 86–2511, Am. Soc. Agric. Eng.

Nofziger, D.L. and Hornsby, A.G., 1986. A microcomputer-based management tool for chemical movement in soil. Appl. Agric. Res., 1: 50–56.

Richard, T. and Steenhuis, T.S., 1988. Tile drain sampling of preferential flow on a field scale. J. Contam. Hydrol., 3: 307–327.

Smettem, K.R.J. and Collis–George, N., 1985. Statistical characterization of soil biopores using a soil peel method. Geoderma, 36: 27–36.

Starr, J.L., Parlange, J.-Y. and Frink, C.R., 1986. Water and chloride movement through a layered field soil. Soil Sci. Soc. Am., 50: 1384–1390.

Steenhuis, T.S. and Naylor, L.M., 1987. A screening method for preliminary assessment of risk to groundwater from land-applied chemicals. J. Contam. Hydrol., 1: 395–406.

Steenhuis, T.S., Pacenka, S. and Porter, K.S., 1987. MOUSE: A management model for evaluating groundwater contamination from diffuse surface sources aided by computer graphics. Appl. Agric. Res., 2: 277–289.

Van Genuchten, M.Th. and Wierenga, P.J., 1986. Solute dispersion coefficients and retardation factors. In, A. Klute (Editor), Methods of Soil Analysis, Part I. Soil Sci. Soc. Am. J., Madison, Wisc., pp. 1025–1054.

Van Ommen, H.C., Dekker, L.W., Dijkama, R., Hulshof, J. and van der Molen, W.H., 1988. A new technique for evaluating the presence of preferential flow paths in non-structured soils. Soil Sci. Soc. Am. J., 55: 1192–1193.